

Gradient recovery for elliptic interface problem: III. Nitsche's method



Hailong Guo, Xu Yang*

Department of Mathematics, University of California, Santa Barbara, CA, 93106, United States

ARTICLE INFO

Article history:

Received 28 September 2017

Received in revised form 22 November 2017

Accepted 24 November 2017

Available online xxxx

Keywords:

Elliptic interface problem

Gradient recovery

Superconvergence

Nitsche's method

Polynomial preserving recovery

ABSTRACT

This is the third paper on the study of gradient recovery for elliptic interface problems. In our previous works Guo and Yang (2017) [23], we developed gradient recovery methods for elliptic interface problems based on body-fitted meshes and immersed finite element methods. Despite the efficiency and accuracy that these methods bring to recover the gradient, there are still some cases in unfitted meshes where skinny triangles appear in the generated local body-fitted triangulations that destroy the accuracy of recovered gradient near the interface. In this paper, we propose a gradient recovery technique based on Nitsche's method for elliptic interface problems, which avoids the loss of accuracy of gradient near the interface caused by skinny triangles. We analyze the supercloseness between the gradient of the numerical solution by the Nitsche's method and the gradient of the interpolation of the exact solution, which leads to the superconvergence of the proposed gradient recovery method. We also present several numerical examples to validate the theoretical results.

© 2017 Elsevier Inc. All rights reserved.

1. Introduction

Elliptic interface problems arise in many applications such as fluid dynamics and materials science, where the background consists of rather different materials on the subdomains separated by smooth curves called interface. The numerical challenge of interface problems comes from the fact that the solution, in general, has low global regularity due to the discontinuity of parameter (e.g. dielectric constant) at the interface. Standard finite element methods have been studied for elliptic interface problems by aligning the triangulation along the interface (body-fitted meshes) and are proven to achieve optimal convergence rates in both L_2 and energy norms [8,3,14,57]. However, when the interface leads to subdomains of complex geometry, it is non-trivial and time-consuming to generate body-fitted meshes.

To overcome the difficulty of mesh generation in the standard finite element methods, tremendous effort has been input to develop numerical methods using unfitted (Cartesian) meshes. [52] is the first to propose the immersed boundary method (IBM) to simulate blood flow using Cartesian meshes. The idea of IBM is to use a Dirac δ -function to model the discontinuity and discretize it to distribute a singular source to nearest grid points [52,53]. But IBM only achieves the first-order accuracy. To improve the accuracy, Leveque and Li characterized the discontinuity as jump conditions and proposed the immersed interface method (IIM) [37]. IIM constructs special finite difference schemes to incorporate the jump conditions near the interface. High order unfitted finite difference methods including matched interface and boundary (MIB) method are also

* Corresponding author.

E-mail addresses: hguo@math.ucsb.edu (H. Guo), xuyang@math.ucsb.edu (X. Yang).

proposed in [63,62]. We refer to [40] for a review on IIM and other unfitted finite difference methods. The ghost fluid method (GFM) is another promising method to solving interface problems as the pioneering work of Liu, Fedkiw, Myungjoo and Kang [45]. GFM is simple and relatively easier to implement since it uses standard finite difference discretization and only needs to modify the right-hand side. This method is only of first-order accuracy, and gets improved in a recent work [21] where a local Voronoi grid is used near the irregular domain's boundary to obtain second-order accurate solutions and first-order accurate gradients. The interested readers are referred to [20] for the recent development on how to impose boundary conditions on an irregular domain in capturing methods, with some applications.

In the meantime, unfitted numerical methods using finite element formulation are also developed for elliptic interface problems. The extended finite element method [7,46,19] enriches the standard continuous finite element space by adding some special basis functions to capture the discontinuity. The immersed finite element methods [38,41,42] modify the basis functions to satisfy the homogeneous jump conditions on interface elements. For the nonconforming immersed finite element method (IFEM) in [41], the numerical solution is continuous inside each element but can be discontinuous on the boundary of each element. Recently, there are also some improved versions of IFEM such as the Petrov–Galerkin IFEM [32, 35,33], symmetric and consistent IFEM [36], and partially penalized IFEM [44].

The Nitsche's method [5,11,12,10,30,27–29,31], also called the cut finite element method, is firstly proposed by Hansbo and Hansbo in [27] to solve elliptic interface problems using unfitted meshes. It is further extended to deal with elastic problems with strong and weak discontinuities [28]. The study of the Nitsche's method for Stokes interface problems can be found in [31]. The key idea of the Nitsche's method is to construct an approximate solution on each fictitious domain and use Nitsche's technique [51] to patch them together. A similar idea was used to develop the fictitious domain method [10,11]. The robust forms of the unfitted Nitsche's method were given in [2,55]. The recent development of the cut finite element method is referred to the review paper [12].

For elliptic interface problems, computation of gradient plays an important role in many practical problems as discussed in [43], which demands numerical methods of high order accuracy. For standard elliptic problems, it is well known that the gradient recovery techniques [64,66,65,60,25,1,50,49,13,58,4] can reconstruct a highly accurate approximate gradient from the primarily computed data with reasonable cost. But for elliptic interface problems, only a few works have been done on the gradient recovery and associated superconvergence theory. For example in [56], a supercloseness result between the gradient of the linear finite element solution and the gradient of the linear interpolation is proved for a two-dimensional interface problem with a body-fitted mesh. For IFEM, Chou et al. introduced two special interpolation formulae to recover flux with high order accuracy for the one-dimensional linear and quadratic IFEM [15,16]. Moreover, Li and his collaborators recently proposed an augmented immersed interface method [43] and a new finite element method [54] to accurately compute the gradient of the solution to elliptic interface problems. In our recent work [22], we proposed an improved polynomial preserving recovery for elliptic interface problems based on a body-fitted mesh and proved the superconvergence on both mildly unstructured meshes and adaptively refined meshes. Later in the two-dimensional case [23], we proposed gradient recovery methods based on symmetric and consistent IFEM [36] and Petrov–Galerkin IFEM [32,34,35] and numerically verified its superconvergence. In [26], we provided a supercloseness result for the partially penalized IFEMs and proved that the recovered gradient using the gradient recovery method in [23] is superconvergent to the exact gradient.

Despite the efficiency and accuracy that the methods mentioned above bring to recover the gradient, there are still some cases in unfitted meshes where skinny triangles appear in the generated local body-fitted triangulations that destroy the accuracy of recovered gradient near the interface. In this paper, we propose an unfitted polynomial preserving recovery (UPPR) based on the Nitsche's method. The key idea is to decompose the domain into two overlapping subdomains, named fictitious domains, by the interface and the triangulation proposed in the Nitsche's method. On each fictitious domain, the standard linear finite element space will be used, and thus the classical polynomial preserving recovery (PPR) can be applied in each fictitious domain. Compared to previous gradient recovery methods [22,23], the new method does not require generating a local body-fitted mesh and therefore avoids the drawback caused by skinny triangles. In general, the exact solutions of the interface problems are piecewise smooth on each subdomain. It implies that the extension of the exact solution on each subdomain to the whole domain is smooth, based on which, the recovered gradient using the interpolation of the exact solution is proven to be superconvergent to the exact gradient at rate of $\mathcal{O}(h^2)$, and this is similar to the classical PPR for standard elliptic problems. In addition, we prove $\mathcal{O}(h^{1.5})$ supercloseness between the gradient given by the Nitsche's method and the gradient of the interpolation of the exact solution by a sharp argument. This enables us to establish the complete superconvergence theory for the proposed UPPR.

The rest of the paper is organized as follows: We introduce briefly the elliptic interface problem and the Nitsche's method in Section 2. In Section 3, we analyze the supercloseness for the Nitsche's method and prove the $\mathcal{O}(h^{1.5})$ supercloseness between the gradient of the finite element solution and the gradient of the interpolation of the exact solution. In section 4, we describe the UPPR for the Nitsche's method and establish its superconvergence theory. In Section 5, we present several numerical examples to confirm our theoretical results.

2. Nitsche's method for elliptic interface problem

In this section, we first introduce the elliptic interface problem and associated notations, and then summarize the unfitted finite element discretization based on Nitsche's method proposed in [2,27] as a preparation for the unfitted polynomial preserving recovery (UPPR) method introduced later.

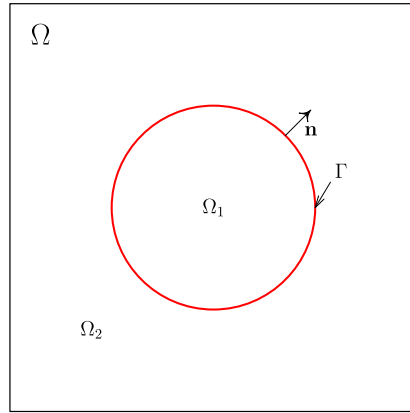


Fig. 1. Typical example of domain Ω with interface Γ .

2.1. Elliptic interface problem

Let Ω be a bounded polygonal domain with Lipschitz boundary $\partial\Omega$ in \mathbb{R}^2 . A C^2 -curve Γ divides Ω into two disjoint subdomains Ω_1 and Ω_2 as in Fig. 1. We consider the following elliptic interface problem

$$-\nabla \cdot (\beta(z)\nabla u(z)) = f(z), \quad \text{in } \Omega_1 \cup \Omega_2, \tag{2.1a}$$

$$u = 0, \quad \text{on } \partial\Omega, \tag{2.1b}$$

$$[[u]] = q, \quad \text{on } \Gamma \tag{2.1c}$$

$$[[\beta \partial_n u]] = g, \quad \text{on } \Gamma \tag{2.1d}$$

where $\partial_n u = (\nabla u) \cdot n$ with n being the unit outward normal vector of Γ and the jump $[[w]]$ on Γ is defined as

$$[[w]] = w_1 - w_2, \tag{2.2}$$

with $w_i = w|_{\Omega_i}$ being the restriction of w on Ω_i . The diffusion coefficient $\beta(z) \geq \beta_0$ is a piecewise smooth function, i.e.

$$\beta(z) = \begin{cases} \beta_1(z) & \text{if } z = (x, y) \in \Omega_1, \\ \beta_2(z) & \text{if } z = (x, y) \in \Omega_2, \end{cases} \tag{2.3}$$

which has a finite jump of function value at the interface Γ .

In this paper, we use the standard notations for Sobolev spaces and their associated norms as in [9,17,18]. For any bounded domain $D \subset \Omega$, the Sobolev space with norm $\|\cdot\|_{k,p,D}$ and seminorm $|\cdot|_{k,p,D}$ is denoted by $W^{k,p}(D)$. When $p = 2$, $W^{k,2}(D)$ is simply denoted by $H^k(D)$ and the subscript p is omitted in its associate norm and seminorm. Similar notations are applied to subdomains of Γ . Let $(\cdot, \cdot)_D$ and $\langle \cdot, \cdot \rangle_\Gamma$ denote the standard L_2 inner products of $L_2(D)$ and $L_2(\Gamma)$, respectively. For a bounded domain $D = D_1 \cup D_2$ with $D_1 \cap D_2 = \emptyset$, let $W^{k,p}(D_1 \cup D_2)$ be the function space consisting of piecewise Sobolev functions w such that $w|_{D_1} \in W^{k,p}(D_1)$ and $w|_{D_2} \in W^{k,p}(D_2)$, whose norm is defined as

$$\|w\|_{k,p,D_1 \cup D_2} = \left(\|w\|_{k,p,D_1}^p + \|w\|_{k,p,D_2}^p \right)^{1/p}, \tag{2.4}$$

and seminorm is defined as

$$|w|_{k,p,D_1 \cup D_2} = \left(|w|_{k,p,D_1}^p + |w|_{k,p,D_2}^p \right)^{1/p}. \tag{2.5}$$

In this paper, we denote C as a generic positive constant which can be different at different occurrences. In addition, it is independent of mesh size and the location of the interface. By $x \lesssim y$, we mean that there exist a constant C such that $x \leq Cy$.

2.2. Nitsche's method

Let \mathcal{T}_h be a triangulation of Ω independent of the location of the interface Γ . For any element $T \in \mathcal{T}_h$, let h_T be the diameter of T and ρ_T be the diameter of the circle inscribed in T . In addition, we make the following assumptions on the triangulation.

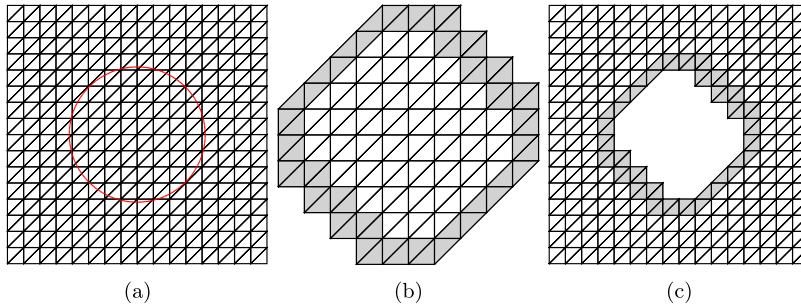


Fig. 2. Triangulation \mathcal{T}_h on the square domain Γ with circular interface Γ : (a) triangulation \mathcal{T}_h ; (b) triangulation $\mathcal{T}_{1,h}$ and $\omega_{1,h}$ (non-shaded triangles); (c) triangulation $\mathcal{T}_{2,h}$ and $\omega_{2,h}$ (non-shaded triangles).

Assumption 2.1. The triangulation \mathcal{T}_h is shape regular in the sense that there is a constant σ such that

$$\frac{h_T}{\rho_T} \leq \sigma, \tag{2.6}$$

for any $T \in \mathcal{T}_h$.

Assumption 2.2. The interface Γ intersects each interface element boundary ∂T exactly twice, and each open edge at most once.

To define the finite element space, denote the set of all elements that intersect the interface Γ by

$$\mathcal{T}_{\Gamma,h} = \{T \in \mathcal{T}_h : \Gamma \cap \bar{T} \neq \emptyset\}, \tag{2.7}$$

and denote the union of all such type elements by

$$\Omega_{\Gamma,h} = \bigcup_{T \in \mathcal{T}_{\Gamma,h}} T. \tag{2.8}$$

Denote the set of all elements covering subdomain Ω_i to be

$$\mathcal{T}_{i,h} = \{T \in \mathcal{T}_h : \overline{\Omega_i} \cap \bar{T} \neq \emptyset\}, \quad i = 1, 2; \tag{2.9}$$

and let

$$\Omega_{i,h} = \bigcup_{T \in \mathcal{T}_{i,h}} T, \quad \omega_{i,h} = \bigcup_{T \in \mathcal{T}_{i,h} \setminus \mathcal{T}_{\Gamma,h}} T, \quad i = 1, 2. \tag{2.10}$$

Fig. 2 gives an illustration of $\Omega_{i,h}$ and $\omega_{i,h}$. We remark that $\Omega_{1,h}$ and $\Omega_{2,h}$ overlap on $\Omega_{\Gamma,h}$, which is shown as the shaded part in Figs. 2b and 2c.

Let $V_{i,h}$ be the standard continuous linear finite element space on $\Omega_{i,h}$, i.e.

$$V_{i,h} = \left\{ v \in C^0(\Omega_{i,h}) : v|_T \in \mathbb{P}_1(T) \text{ for any } T \in \mathcal{T}_{i,h} \right\}, \quad i = 1, 2, \tag{2.11}$$

where $\mathbb{P}_k(T)$ is the space of polynomials with degree $\leq k$ on T . Then, we define the finite element space V_h as

$$V_h = \left\{ v_h = (v_{1,h}, v_{2,h}) : v_{i,h} \in V_{i,h}, i = 1, 2 \right\}, \tag{2.12}$$

and $V_{h,0}$ as

$$V_{h,0} = \{v_h \in V_h : v_h|_{\partial\Omega} = 0\}. \tag{2.13}$$

Note that a function in V_h is a vector-valued function from $\mathbb{R}^2 \mapsto \mathbb{R}^2$, which has a zero component in $\omega_{1,h} \cup \omega_{2,h}$ but in general two non-zero components in $\mathcal{T}_{\Gamma,h}$. It means that one will have two sets of basis functions for any element T in $\mathcal{T}_{\Gamma,h}$: one for $V_{1,h}$ and the other for $V_{2,h}$.

For any T in $\mathcal{T}_{\Gamma,h}$, denote $T_i = T \cap \Omega_i$ as the part of T in Ω_i , with $|T_i|$ being the measure of T_i in \mathbb{R}^2 . Denote $\Gamma_T = \Gamma \cap T$ as the part of Γ in T , with $|\Gamma_T|$ being the measure of Γ_T in \mathbb{R}^1 . To increase the robustness of the Nitsche's method, we introduce two weights as used in [2]

$$\kappa_1|_T = \frac{\beta_2|T_1|}{\beta_2|T_1| + \beta_1|T_2|}, \quad \kappa_2|_T = \frac{\beta_1|T_2|}{\beta_2|T_1| + \beta_1|T_2|}, \tag{2.14}$$

which satisfies that $\kappa_1 + \kappa_2 = 1$. Then, we define the weighted averaging of a function v_h in V_h on the interface Γ as

$$\{\mathbf{w}\} = \kappa_1 v_{1,h} + \kappa_2 v_{2,h}, \quad \{\mathbf{w}\}^* = \kappa_2 v_{1,h} + \kappa_1 v_{2,h}. \tag{2.15}$$

Using the notations introduced above, the Nitsche's method [12,27,2] for the elliptic interface problem (2.1) is to find $u_h \in V_{h,0}$ such that

$$a_h(u_h, v_h) = L_h(v_h), \quad \forall v_h \in V_{h,0}; \tag{2.16}$$

where the bilinear form a_h is defined as

$$a_h(u_h, v_h) = \sum_{i=1}^2 (\beta \nabla u_{i,h}, \nabla v_{i,h})_{\Omega_i} - \langle \llbracket u_h \rrbracket, \llbracket \beta \partial_n v_h \rrbracket \rangle_{\Gamma} - \langle \llbracket v_h \rrbracket, \llbracket \beta \partial_n u_h \rrbracket \rangle_{\Gamma} + h^{-1} \langle \gamma \llbracket u_h \rrbracket, \llbracket v_h \rrbracket \rangle_{\Gamma}, \tag{2.17}$$

and the linear functional L_h is defined as

$$L_h(v_h) = \sum_{i=1}^2 (f, \nabla v_{i,h})_{\Omega_i} - \langle q, \llbracket \beta \partial_n v_h \rrbracket \rangle_{\Gamma} + \langle \gamma q, \llbracket v_h \rrbracket \rangle_{\Gamma} + \langle g, \{\mathbf{w}\}^* \rangle_{\Gamma}, \tag{2.18}$$

with the stability parameter

$$\gamma|_T = \frac{2h_T |\Gamma_T|}{|T_1|/\beta_1 + |T_2|/\beta_2}. \tag{2.19}$$

In [2], the discrete variational form is shown to be consistent as the following theorem:

Theorem 2.3. *Let u be the solution of the interface problem (2.1). Then we have*

$$a_h(\tilde{u}, v_h) = L(v_h), \quad \forall v_h \in V_{h,0}, \tag{2.20}$$

where $\tilde{u} = (u_1, u_2)$ with the short-hand notation $u_i = u|_{\Omega_i}$ as used in (2.2).

Theorem 2.3 implies the following Galerkin orthogonality:

Corollary 2.4. *Let u be the solution of (2.1) and u_h be the solution of the discrete problem (2.16). Then we have*

$$a_h(\tilde{u} - u_h, v_h) = 0, \quad \forall v_h \in V_{h,0}, \tag{2.21}$$

with $\tilde{u} = (u_1, u_2)$.

To analyze the stability of the bilinear form $a_h(\cdot, \cdot)$, we introduce the following mesh-dependent norm [12,27]

$$\|v\|_h^2 = \|\nabla v\|_{0,\Omega_1 \cup \Omega_2}^2 + \sum_{T \in \mathcal{T}_{\Gamma,h}} h_T \|\llbracket \partial_n v \rrbracket\|_{0,\Gamma_T}^2 + \sum_{T \in \mathcal{T}_{\Gamma,h}} h_T^{-1} \|\llbracket v \rrbracket\|_{0,\Gamma_T}^2. \tag{2.22}$$

In [27], it is shown that the bilinear form $a_h(\cdot, \cdot)$ is coercive with respect to the above mesh-dependent norm in the following sense

Theorem 2.5. *There is a constant C such that*

$$C \|v_h\|_h^2 \leq a_h(v_h, v_h), \quad \forall v_h \in V_h. \tag{2.23}$$

Based on the above coercivity, Hansbo et al. proved the following optimal convergence result [27]:

Theorem 2.6. *Let u be the solution to the interface problem (2.1) and u_h be the finite element solution to (2.16). If $u \in H^2(\Omega_1 \cup \Omega_2)$, then*

$$\|\tilde{u} - u_h\|_h \leq Ch \|u\|_{2,\Omega_1 \cup \Omega_2}, \tag{2.24}$$

and

$$\|\tilde{u} - u_h\|_{0,\Omega} \leq Ch^2 \|u\|_{2,\Omega_1 \cup \Omega_2}, \tag{2.25}$$

with $\tilde{u} = (u_1, u_2)$.

3. Supercloseness analysis

In this section, we establish the supercloseness result between the gradient of the finite element solution and the gradient of the interpolation of the exact solution as a preparation for the superconvergence analysis of the unfitted polynomial preserving recovery based on Nitsche’s method. For that propose, we need the triangulation \mathcal{T}_h to satisfy Condition (σ, α) as explained below.

Two adjacent triangles are said to form an $\mathcal{O}(h^{1+\alpha})$ approximate parallelogram if the lengths of any two opposite edges differ only by $\mathcal{O}(h^{1+\alpha})$.

Definition 3.1. The triangulation \mathcal{T}_h is called to satisfy Condition (σ, α) if there exist a partition $\mathcal{T}_h^1 \cup \mathcal{T}_h^2$ of \mathcal{T}_h and positive constants α and σ such that every two adjacent triangles in \mathcal{T}_h^1 form an $\mathcal{O}(h^{1+\alpha})$ parallelogram and

$$\sum_{T \in \mathcal{T}_h^2} |T| = \mathcal{O}(h^\sigma).$$

Remark 3.1. For the Nitsche’s method, we usually use a Cartesian mesh which is independent of the location of the interface. Therefore the mesh satisfies Condition (σ, α) with $\sigma = \infty$ and $\alpha = 1$.

To define the interpolation operator, we need to extend the function defined on the subdomain Ω_i to the whole domain Ω . Let $E_i, i = 1, 2$, be the H^3 -extension operator from $H^3(\Omega_i)$ to $H^3(\Omega)$ such that

$$(E_i w)|_{\Omega_i} = w, \tag{3.1}$$

and

$$\|E_i w\|_{s, \Omega} \leq C \|w\|_{s, \Omega_i}, \quad \forall w \in H^s(\Omega_i), \quad s = 0, 1, 2, 3. \tag{3.2}$$

Let $I_{i,h}$ be the standard nodal interpolation operator from $C(\bar{\Omega})$ to $V_{i,h}$. Define the interpolation operator for the finite element space V_h as

$$I_h^* v = (I_{1,h}^* v_1, I_{1,h}^* v_2), \tag{3.3}$$

where

$$I_{i,h}^* = I_{i,h} E_i v_i, \quad i = 1, 2. \tag{3.4}$$

Optimal approximation capability of I_h^* is proved in [27]. Assume \mathcal{T}_h satisfies Condition (σ, α) , and then we can prove the following theorem:

Theorem 3.2. Suppose the triangulation \mathcal{T}_h satisfies Condition (σ, α) . Let u be the solution of the interface problem (2.1) and $I_h^* u$ be the interpolation of u in the finite element space $V_{h,0}$. If $u \in H^1(\Omega) \cap H^3(\Omega_1 \cup \Omega_2) \cap W^{2,\infty}(\Omega_1 \cup \Omega_2)$, then for $\tilde{u} = (u_1, u_2)$ and all $v_h \in V_{h,0}$,

$$a_h(\tilde{u} - I_h^* u, v_h) \leq C \left(h^{1+\rho} (\|u\|_{3, \Omega_1 \cup \Omega_2} + \|u\|_{2, \infty, \Omega_1 \cup \Omega_2}) + h^{3/2} \|u\|_{2, \infty, \Omega_1 \cup \Omega_2} \right) |v_h|_h, \tag{3.5}$$

where $\rho = \min(\alpha, \frac{\sigma}{2}, \frac{1}{2})$.

Proof. By (2.17), we have

$$\begin{aligned} a_h(\tilde{u} - I_h^* u, v_h) &= \sum_{i=1}^2 \left(\beta \nabla(u_i - I_{i,h}^* u_i), \nabla v_{i,h} \right)_{\Omega_i} - \langle [u - I_h^* u], \llbracket \beta \partial_n v_h \rrbracket \rangle_{\Gamma} \\ &\quad - \langle \llbracket v_h \rrbracket, \llbracket \beta \partial_n (u - I_h^* u) \rrbracket \rangle_{\Gamma} + h^{-1} \langle \gamma [u - I_h^* u], \llbracket v_h \rrbracket \rangle_{\Gamma} \\ &\leq \left| \langle \beta \nabla(u_1 - I_{1,h}^* u_1), \nabla v_{1,h} \rangle_{\omega_{1,h}} \right| + \left| \langle \beta \nabla(u_2 - I_{2,h}^* u_2), \nabla v_{2,h} \rangle_{\omega_{2,h}} \right| \\ &\quad + \left| \langle \beta \nabla(u - I_h^* u), \nabla v_h \rangle_{\Omega_{\Gamma,h}} \right| + \left| \langle [u - I_h^* u], \llbracket \beta \partial_n v_h \rrbracket \rangle_{\Gamma} \right| \\ &\quad + \left| \langle \llbracket v_h \rrbracket, \llbracket \beta \partial_n (u - I_h^* u) \rrbracket \rangle_{\Gamma} \right| + h^{-1} \left| \langle \gamma [u - I_h^* u], \llbracket v_h \rrbracket \rangle_{\Gamma} \right| \\ &:= F_1 + F_2 + F_3 + F_4 + F_5 + F_6, \end{aligned} \tag{3.6}$$

because $\Omega_i \subset \omega_{1,h} \cup \Omega_{\Gamma,h}$ for $i = 1, 2$. Since \mathcal{T}_h satisfies Condition (σ, α) , it follows that $\mathcal{T}_{1,h} \setminus \mathcal{T}_{\Gamma,h}$ and $\mathcal{T}_{2,h} \setminus \mathcal{T}_{\Gamma,h}$ also satisfy Condition (σ, α) . Notice that the restriction of the finite element space $V_{i,h}$ on $\omega_{i,h}$ is just the standard continuous linear finite element space for $i = 1, 2$. Then by Lemma 2.1 in [58], we have

$$|F_1| \leq Ch^{1+\rho} (\|u\|_{3,\Omega_1} + \|u\|_{2,\infty,\Omega_1}) |v_h|_h, \tag{3.7}$$

$$|F_2| \leq Ch^{1+\rho} (\|u\|_{3,\Omega_2} + \|u\|_{2,\infty,\Omega_2}) |v_h|_h, \tag{3.8}$$

where $\rho = \min(\alpha, \frac{\sigma}{2}, \frac{1}{2})$. To estimate F_3 , the Cauchy–Schwartz inequality implies

$$\begin{aligned} F_3 &\leq \left(\sum_{T \in \mathcal{T}_{\Gamma,h}} \|\nabla(u_1 - I_{1,h}^* u_1)\|_{0,T_1}^2 \right)^{1/2} \left(\sum_{T \in \mathcal{T}_{\Gamma,h}} \|\nabla v_{1,h}\|_{0,T_1}^2 \right)^{1/2} \\ &\quad + \left(\sum_{T \in \mathcal{T}_{\Gamma,h}} \|\nabla(u_2 - I_{1,h}^* u_2)\|_{0,T_2}^2 \right)^{1/2} \left(\sum_{T \in \mathcal{T}_{\Gamma,h}} \|\nabla v_{2,h}\|_{0,T_2}^2 \right)^{1/2} \\ &\leq C \left(\sum_{T \in \mathcal{T}_{\Gamma,h}} h^4 \|u\|_{2,\infty,\Omega_1}^2 \right)^{1/2} \left(\sum_{T \in \mathcal{T}_{\Gamma,h}} \|\nabla v_{1,h}\|_{0,T_1}^2 \right)^{1/2} \\ &\quad + C \left(\sum_{T \in \mathcal{T}_{\Gamma,h}} h^4 \|u\|_{2,\infty,\Omega_2}^2 \right)^{1/2} \left(\sum_{T \in \mathcal{T}_{\Gamma,h}} \|\nabla v_{2,h}\|_{0,T_2}^2 \right)^{1/2} \\ &\leq Ch^2 \|u\|_{2,\infty,\Omega_1} \left(\sum_{T \in \mathcal{T}_{\Gamma,h}} 1 \right)^{1/2} \left(\sum_{T \in \mathcal{T}_{\Gamma,h}} \|\nabla v_{1,h}\|_{0,T_1}^2 \right)^{1/2} \\ &\quad + Ch^2 \|u\|_{2,\infty,\Omega_2} \left(\sum_{T \in \mathcal{T}_{\Gamma,h}} 1 \right)^{1/2} \left(\sum_{T \in \mathcal{T}_{\Gamma,h}} \|\nabla v_{2,h}\|_{0,T_2}^2 \right)^{1/2} \\ &\leq Ch^{3/2} \|u\|_{2,\infty,\Omega_1} |v|_{1,\Omega_1} + Ch^{3/2} \|u\|_{2,\infty,\Omega_2} |v|_{1,\Omega_2} \\ &\leq Ch^{3/2} \|u\|_{2,\infty,\Omega_1 \cup \Omega_2} |v|_{1,\Omega_1 \cup \Omega_2}; \end{aligned}$$

where we have used the fact $\sum_{T \in \mathcal{T}_{\Gamma,h}} 1 \approx \mathcal{O}(h^{-1})$. By the Cauchy–Schwartz inequality and the trace inequality in [27,55], we have

$$\begin{aligned} F_4 &\leq \left(\sum_{T \in \mathcal{T}_{\Gamma,h}} h_T^{-1} \|\llbracket u - I_h^* u \rrbracket\|_{0,\Gamma_T}^2 \right)^{\frac{1}{2}} \left(\sum_{T \in \mathcal{T}_{\Gamma,h}} h_T \|\llbracket \beta \partial_n v_h \rrbracket\|_{0,\Gamma_T}^2 \right)^{\frac{1}{2}} \\ &\leq \left(\sum_{T \in \mathcal{T}_{\Gamma,h}} \sum_{i=1}^2 h_T^{-1} \|u_i - I_{i,h}^* u_i\|_{0,\Gamma_T}^2 \right)^{\frac{1}{2}} \|v_h\|_h \\ &\leq C \left(\sum_{T \in \mathcal{T}_{\Gamma,h}} \sum_{i=1}^2 (h_T^{-2} \|u_i - I_{i,h}^* u_i\|_{0,T}^2 + \|\nabla(u_i - I_{i,h}^* u_i)\|_{0,T}^2) \right)^{\frac{1}{2}} \|v_h\|_h \tag{3.9} \\ &\leq C \left(\sum_{T \in \mathcal{T}_{\Gamma,h}} \sum_{i=1}^2 h_T^4 \|E_i u_i\|_{2,\infty,T}^2 \right)^{\frac{1}{2}} \|v_h\|_h \\ &\leq Ch^2 \|u\|_{2,\infty,\Omega_1 \cup \Omega_2} \left(\sum_{T \in \mathcal{T}_{\Gamma,h}} 1 \right)^{\frac{1}{2}} \|v_h\|_h \\ &\leq Ch^{3/2} \|u\|_{2,\infty,\Omega_1 \cup \Omega_2} \|v_h\|_h. \end{aligned}$$

Similarly, we can estimate F_5 and F_6 as

$$\begin{aligned} F_5 &\leq Ch^{3/2} \|u\|_{2,\infty,\Omega_1\cup\Omega_2} \|v_h\|_h; \\ F_6 &\leq Ch^{3/2} \|u\|_{2,\infty,\Omega_1\cup\Omega_2} \|v_h\|_h. \end{aligned} \tag{3.10}$$

Combing all the above estimations, we get (3.5). \square

Now we state our main supercloseness result as follows.

Theorem 3.3. Assume the same hypothesis as in Theorem 3.2 and let u_h be the finite element solution of the discrete variational problem (2.16), then

$$\|u_h - I_h^* u\|_h \leq C \left(h^{1+\rho} (\|u\|_{3,\Omega_1\cup\Omega_2} + \|u\|_{2,\infty,\Omega_1\cup\Omega_2}) + h^{3/2} \|u\|_{2,\infty,\Omega_1\cup\Omega_2} \right), \tag{3.11}$$

where $\rho = \min(\alpha, \frac{\alpha}{2}, \frac{1}{2})$.

Proof. By Corollary 2.4, we have the following Galerkin orthogonality

$$a_h(\tilde{u} - u_h, v_h) = 0, \quad \forall v_h \in V_h, 0,$$

where $\tilde{u} = (u_1, u_2)$. Then we have

$$a_h(u_h - I_h^* u, v_h) = a_h(\tilde{u} - I_h^* u, v_h), \quad \forall v_h \in V_h, 0.$$

Taking $v_h = u_h - I_h^* u$ and using Theorem 3.2 and Theorem 2.5, we prove (3.11). \square

Remark 3.2. Theorem 3.3 implies that we can have the same supercloseness result as the partially penalized IFEM [26].

4. Superconvergent gradient recovery

In this section, we first propose the unfitted polynomial preserving recovery (UPPR) technique based on the Nitsche's method, then prove that the recovered gradient by UPPR is superconvergent to the exact gradient on mildly unstructured meshes.

4.1. Unfitted polynomial preserving recovery

To accurately recover the gradient, we notice that the finite element solution u_h of the Nitsche's method (2.16) consists of two part: $u_{1,h}$ and $u_{2,h}$. Also, by the fact that we can smoothly extend the exact solution $u|_{\Omega_i}$ ($i = 1, 2$) to the whole domain, it is safe to assume $u|_{\Omega_i}$ and its extension $E_i u|_{\Omega_i}$ is smooth in general. For each $i \in \{1, 2\}$, $u_{i,h} \in V_h$ is a continuous piecewise polynomial on fictitious domain $\Omega_{i,h}$ but its gradient $\nabla u_{i,h}$ is only a piecewise constant function. This motivates us to naturally use some smoothing operators such as superconvergent patch recovery (SPR) and polynomial preserving recovery (PPR) to smooth the discontinuous gradient into a continuous one on each fictitious domain $\Omega_{i,h}$.

To this end, let G_h^i be the PPR gradient recovery operator [60,50] on the fictitious domain $\Omega_{i,h}$ for $i = 1, 2$. Then G_h^i is a linear operator from $V_{i,h}$ to $V_{i,h} \times V_{i,h}$ whose value at each nodal point is obtained by the local least squares fitting using sampling points only located in $\Omega_{i,h}$. According to [24,60,50], the gradient recovery operator G_h^i is bounded in the sense that

$$\|G_h^i v_{i,h}\|_{0,\Omega_{i,h}} \lesssim |v_{i,h}|_{1,\Omega_{i,h}}, \quad v_{i,h} \in V_{i,h}, \tag{4.1}$$

and is consistent in following sense that

$$\|\nabla v_i - G_h I_{i,h} v_i\|_{0,\Omega} \lesssim h^2 \|v_i\|_{3,\Omega_{i,h}}, \quad \forall v_i \in H^3(\Omega_{i,h}), \tag{4.2}$$

for $i = 1, 2$.

Let u_h be the finite element solution of the discrete variational problem (2.16). We define the recovered gradient of u_h as

$$R_h u_h = \left(G_h^1 u_{1,h}, G_h^2 u_{2,h} \right). \tag{4.3}$$

The linearity of G_h^i implies R_h is a linear operator from V_h to $V_h \times V_h$. R_h is called the unfitted polynomial preserving recovery (UPPR).

Remark 4.1. The definition of the gradient recovery operator can be presented in a more general form. In fact, G_h^i can be chosen as any local gradient recovery operators [59] like simple averaging, weight averaging, SPR and PPR. For simplicity and efficiency, we only consider G_h^i as PPR here.

Remark 4.2. The main idea is to use the standard PPR on each fictitious domain $\Omega_{i,h}$, which is similar to the improved polynomial preserving recovery for the finite element method based on body-fitted meshes [22]. But the proposed method (4.3) does not require the mesh fitting the interface, and that is why we call it unfitted polynomial preserving recovery method.

Remark 4.3. We considered the gradient recovery technique for immersed finite element methods in [23], which is also based on unfitted meshes. The gradient recovery technique in [23] needs to generate a local body-fitted mesh by dividing every interface triangle into three sub-triangles, which can lead to skinny triangles and therefore a loss of accuracy. The proposed gradient recovery operator (4.3) overcomes this drawback.

Note that as a function in $V_h \times V_h$, $R_h u_h$ is continuous on each subdomain Ω_i and is discontinuous in the whole domain Ω which approximates the exact gradient ∇u . Also, similar to the finite element solution u_h , both $G_h^1 u_{1,h}$ and $G_h^2 u_{2,h}$ in (4.3) are, in general, non-zero on interface triangles $T \in \mathcal{T}_{h,\Gamma}$. For the gradient recovery operator R_h (4.3), we can show that it is consistent as follows:

Theorem 4.1. Let $R_h : V_h \rightarrow V_h \times V_h$ be the unfitted polynomial preserving recovery operator defined in (4.3) and I_h^* be the interpolation of u into the finite element space V_h as defined in (3.3). If $u \in H^3(\Omega_1 \cup \Omega_2)$, then we have

$$\|\tilde{\nabla} u - R_h I_h^* u\|_{0,\Omega_1 \cup \Omega_2} \leq Ch^2 |u|_{3,\Omega_1 \cup \Omega_2}, \quad (4.4)$$

with $\tilde{\nabla} u = (\nabla u_1, \nabla u_2)$.

Proof. By (2.4), (3.3), (3.4), and (4.2), we have

$$\begin{aligned} \|\tilde{\nabla} u - R_h I_h^* u\|_{0,\Omega_1 \cup \Omega_2}^2 &= \|\nabla u_1 - G_h^1 I_{1,h}^* u\|_{0,\Omega_1}^2 + \|\nabla u_2 - G_h^2 I_{2,h}^* u\|_{0,\Omega_2}^2 \\ &= \|\nabla E_1 u_1 - G_h^1 I_{1,h}^* u\|_{0,\Omega_1}^2 + \|\nabla E_2 u_2 - G_h^2 I_{2,h}^* u\|_{0,\Omega_2}^2 \\ &\leq \|\nabla E_1 u_1 - G_h^1 I_{1,h}^* u\|_{0,\Omega_{1,h}}^2 + \|\nabla E_2 u_2 - G_h^2 I_{2,h}^* u\|_{0,\Omega_{2,h}}^2 \\ &= \|\nabla E_1 u_1 - G_h^1 I_{1,h}^* E_1 u\|_{0,\Omega_{1,h}}^2 + \|\nabla E_2 u_2 - G_h^2 I_{2,h}^* E_2 u\|_{0,\Omega_{2,h}}^2 \\ &\leq C_1 h^4 |E_1 u_1|_{3,\Omega_{1,h}}^2 + C_2 h^4 |E_2 u_2|_{3,\Omega_{2,h}}^2 \\ &\leq C_1 h^4 |u_1|_{3,\Omega_1}^2 + C_2 h^4 |u_2|_{3,\Omega_2}^2 \\ &\leq Ch^4 |u|_{3,\Omega_1 \cup \Omega_2}^2. \end{aligned} \quad (4.5)$$

Taking square root on both sides of (4.5) completes our proof. \square

Remark 4.4. Theorem 4.1 means the recovered gradient using the interpolation of the exact solution is superconvergent to the exact gradient at a rate of $\mathcal{O}(h^2)$. It is similar to the classical PPR operator for regular elliptic problems.

4.2. Superconvergence analysis

In the following, we shall show the superconvergence property of the proposed UPPR. Our main superconvergent tool is the supercloseness result provided in Section 3.

Theorem 4.2. Under the same hypothesis as in Theorem 3.2. We further assume that u_h is the finite element solution of the discrete variational problem (2.16). Then we have

$$\|\tilde{\nabla} u - R_h u_h\|_{0,\Omega_1 \cup \Omega_2} \leq C \left(h^{1+\rho} (\|u\|_{3,\Omega_1 \cup \Omega_2} + \|u\|_{2,\infty,\Omega_1 \cup \Omega_2}) + h^{3/2} \|u\|_{2,\infty,\Omega_1 \cup \Omega_2} \right),$$

where $\tilde{\nabla} u = (\nabla u_1, \nabla u_2)$ and $\rho = \min(\alpha, \frac{\alpha}{2}, \frac{1}{2})$.

Proof. By the triangle inequality, we have

$$\|\tilde{\nabla} u - R_h u_h\|_{0,\Omega_1 \cup \Omega_2} \leq \|\tilde{\nabla} u - R_h I_h^* u\|_{0,\Omega_1 \cup \Omega_2} + \|R_h I_h^* u - R_h u_h\|_{0,\Omega_1 \cup \Omega_2} := F_1 + F_2.$$

According to Theorem 4.1, we have

$$F_1 \leq Ch^2 |u|_{3,\Omega_1 \cup \Omega_2}.$$

For F_2 , we have

$$\begin{aligned}
 F_2^2 &= \|G_h^1 I_{1,h}^* u_1 - G_h^1 u_{1,h}\|_{0,\Omega_1}^2 + \|G_h^2 I_{2,h}^* u_2 - G_h^2 u_{2,h}\|_{0,\Omega_2}^2 \\
 &\leq \|G_h^1 I_{1,h}^* u_1 - G_h^1 u_{1,h}\|_{0,\Omega_{1,h}}^2 + \|G_h^2 I_{2,h}^* u_2 - G_h^2 u_{2,h}\|_{0,\Omega_{2,h}}^2 \\
 &\leq C \|\nabla(I_{1,h}^* u_1 - u_{1,h})\|_{0,\Omega_{1,h}}^2 + C \|\nabla(I_{2,h}^* u_2 - u_{2,h})\|_{0,\Omega_{2,h}}^2 \\
 &\leq C \|\nabla(I_{1,h}^* u_1 - u_{1,h})\|_{0,\Omega_1}^2 + C \|\nabla(I_{2,h}^* u_2 - u_{2,h})\|_{0,\Omega_2}^2 + C \|\nabla(I_{1,h}^* u_1 - u_{1,h})\|_{0,\Omega_{\Gamma,h}}^2 + C \|\nabla(I_{2,h}^* u_2 - u_{2,h})\|_{0,\Omega_{\Gamma,h}}^2 \\
 &= C \|\nabla(I_h^* u - u_h)\|_{0,\Omega_1 \cup \Omega_2}^2 + C \|\nabla(I_{1,h}^* u_1 - u_{1,h})\|_{0,\Omega_{1,h} \setminus \Omega_1}^2 + C \|\nabla(I_{2,h}^* u_2 - u_{2,h})\|_{0,\Omega_{1,h} \setminus \Omega_2}^2 \\
 &= C \|u_h - I_h^* u\|_h^2 + C \|\nabla(I_{1,h}^* u_1 - u_{1,h})\|_{0,\Omega_{1,h} \setminus \Omega_1}^2 + C \|\nabla(I_{2,h}^* u_2 - u_{2,h})\|_{0,\Omega_{1,h} \setminus \Omega_2}^2 \\
 &:= F_3 + F_4 + F_5.
 \end{aligned}$$

Theorem 3.3 implies that

$$F_3 \leq C \left(h^{1+\rho} (\|u\|_{3,\Omega_1 \cup \Omega_2} + \|u\|_{2,\infty,\Omega_1 \cup \Omega_2}) + h^{3/2} \|u\|_{2,\infty,\Omega_1 \cup \Omega_2} \right)^2.$$

Then, we estimate F_4 as

$$\begin{aligned}
 F_4 &\leq C \|\nabla(I_{1,h}^* u_1 - u_{1,h})\|_{0,\Omega_{1,h} \setminus \Omega_1}^2 \\
 &\leq C \|\nabla(I_{1,h}^* u_1 - u_{1,h})\|_{0,\Omega_{\Gamma,h}}^2 \\
 &\leq C \|\nabla(I_{1,h} E_1 u_1 - u_{1,h})\|_{0,\Omega_{\Gamma,h}}^2 \\
 &= C \sum_{T \in \mathcal{T}_{\Gamma,h}} \|\nabla(I_{1,h} E_1 u_1 - u_{1,h})\|_{0,T}^2 \\
 &\leq C \sum_{T \in \mathcal{T}_{\Gamma,h}} h^4 |E_1 u_1|_{2,\infty,T} \\
 &\leq C h^4 |u|_{2,\infty,\Omega_1 \cup \Omega_2} \sum_{T \in \mathcal{T}_{\Gamma,h}} 1 \\
 &\leq C h^3 |u|_{2,\infty,\Omega_1 \cup \Omega_2},
 \end{aligned}$$

where we have used the fact $\sum_{T \in \mathcal{T}_{\Gamma,h}} 1 \approx \mathcal{O}(h^{-1})$. Similarly, we have

$$F_5 \leq C h^3 |u|_{2,\infty,\Omega_1 \cup \Omega_2}.$$

Combining the estimates for F_3 , F_4 , and F_5 , we have

$$F_2 \leq C \left(h^{1+\rho} (\|u\|_{3,\Omega_1 \cup \Omega_2} + \|u\|_{2,\infty,\Omega_1 \cup \Omega_2}) + h^{3/2} \|u\|_{2,\infty,\Omega_1 \cup \Omega_2} \right),$$

which completes the proof. \square

By the above superconvergence result, we naturally define a local *a posteriori* error estimator on an element $T \in \mathcal{T}_h$:

$$\eta_T = \|\beta^{1/2} (R_h u_h - \nabla u_h)\|_{0,T}, \tag{4.6}$$

and the corresponding global error estimator

$$\eta_h = \left(\sum_{T \in \mathcal{T}_h} \eta_T^2 \right)^{1/2}. \tag{4.7}$$

Theorem 4.2 implies the error estimator (4.6) (or (4.7)) is asymptotically exact for the Nitsche’s method:

Theorem 4.3. Assume the same hypothesis in Theorem 3.2 and let u_h be the finite element solution of the discrete variational problem (2.16). Further assume that there is a constant $C(u) > 0$ such that

$$\|\tilde{\nabla} u - \nabla u_h\|_{0,\Omega} \geq C(u)h, \tag{4.8}$$

then it holds that

$$\left| \frac{\eta_h}{\|\beta^{1/2} (\tilde{\nabla} u - \nabla u_h)\|_{0,\Omega}} - 1 \right| \leq Ch^\rho, \tag{4.9}$$

where $\tilde{\nabla} u = (\nabla u_1, \nabla u_2)$ and $\rho = \min(\alpha, \frac{\alpha}{2}, \frac{1}{2})$.

Table 1
Numerical results for Example 5.1 with $\beta_1 = 10, \beta_2 = 1$.

h	De	Order	$D^i e$	Order	$D^r e$	Order
1/16	4.61e-02	-	2.37e-02	-	1.82e-02	-
1/32	2.34e-02	0.98	9.34e-03	1.34	7.70e-03	1.25
1/64	1.17e-02	1.00	3.28e-03	1.51	2.75e-03	1.48
1/128	5.88e-03	1.00	1.17e-03	1.48	9.95e-04	1.47
1/256	2.94e-03	1.00	4.08e-04	1.52	3.36e-04	1.56
1/512	1.47e-03	1.00	1.43e-04	1.51	1.17e-04	1.53
1/1024	7.35e-04	1.00	5.08e-05	1.49	4.17e-05	1.48

Table 2
Numerical results for Example 5.1 with $\beta_1 = 1000, \beta_2 = 1$.

h	De	Order	$D^i e$	Order	$D^r e$	Order
1/16	4.19e-02	-	2.62e-02	-	2.15e-02	-
1/32	2.13e-02	0.98	9.98e-03	1.39	8.52e-03	1.33
1/64	1.06e-02	1.00	3.53e-03	1.50	3.09e-03	1.46
1/128	5.33e-03	1.00	1.25e-03	1.50	1.12e-03	1.47
1/256	2.66e-03	1.00	4.33e-04	1.52	3.75e-04	1.57
1/512	1.33e-03	1.00	1.52e-04	1.51	1.29e-04	1.54
1/1024	6.66e-04	1.00	5.41e-05	1.49	4.59e-05	1.49

Proof. By Theorem 4.2 and (4.8), we have

$$\left| \frac{\eta_h}{\beta^{1/2} \|\tilde{\nabla} u - \nabla u_h\|_{0,\Omega}} - 1 \right| \leq \left| \frac{\|\beta^{1/2}(R_h u_h - \tilde{\nabla} u)\|_{0,\Omega}}{\|\beta^{1/2}(\tilde{\nabla} u - \nabla u_h)\|_{0,\Omega}} \right| \leq Ch^\rho. \quad \square \tag{4.10}$$

Remark 4.5. For interface problems, there are two types of errors: the error introduced by geometric discretization and the error introduced by the singularity of the solution. The first type of error can be predicted by the curvature of the interface [56,61]. The error estimator (4.6) or (4.7) can be used to estimate the second type of error.

5. Numerical examples

In this section, we show the performance of proposed unfitted polynomial preserving recovery (UPPR) method by several numerical examples with both simple and complex interface geometries. The computational domains of all examples are chosen as $\Omega = (-1, 1) \times (-1, 1)$. For the first three numerical examples, the uniform triangulations of Ω are obtained by dividing Ω into N^2 sub-squares and then dividing each sub-square into two right triangles. The resulted uniform mesh size is $h = \frac{2}{N}$. For convenience, we use the following errors in all the examples:

$$De := \|\tilde{\nabla} u - \nabla u_h\|_{0,\Omega_1 \cup \Omega_2}, \quad D^i e := \|\nabla I_h^* u - \nabla u_h\|_{0,\Omega_1 \cup \Omega_2},$$

$$D^r e := \|\tilde{\nabla} u - R_h u_h\|_{0,\Omega_1 \cup \Omega_2},$$

with $\tilde{\nabla} u = (\nabla u_1, \nabla u_2)$.

Example 5.1. In this example, we consider the interface problem (2.1) with homogeneous jump condition as in [41]. The interface is a circular interface of radius $r_0 = 0.5$. The exact solution is

$$u(x, y) = \begin{cases} \frac{r^3}{\beta_1} & \text{if } (x, y) \in \Omega_1, \\ \frac{r^3}{\beta_2} + \left(\frac{1}{\beta^-} - \frac{1}{\beta^+}\right)r_0^3 & \text{if } (x, y) \in \Omega_2, \end{cases}$$

where $r = \sqrt{x^2 + y^2}$.

We consider the following four typical different jump ratios: $\beta_1/\beta_2 = 1/10$ (moderate jump), $\beta_1/\beta_2 = 1/1000$ (large jump), $\beta_1/\beta_2 = 1/100000$ (huge jump), and $\beta_1/\beta_2 = 100000$ (huge jump). The numerical errors are displayed in Tables 1–4. We observe an optimal convergence in the H^1 -seminorm as predicted by Theorem 2.6. The observed $\mathcal{O}(h^{1.5})$ supercloseness and superconvergence confirm our theoretical results. In addition, we observe the same superconvergence results in all different cases. It means that the superconvergence results are independent of the jump ratios of the coefficient. In Fig. 3, we plot the recovered gradient on the initial mesh.

Example 5.2. In this example, we consider the flower-shape interface problem with non-homogeneous jump conditions as studied in [47,62]. The interface curve Γ in polar coordinates is given by

Table 3
Numerical results for Example 5.1 with $\beta_1 = 1, \beta_2 = 100000$.

h	De	Order	$D^i e$	Order	$D^r e$	Order
1/16	1.99e-01	-	2.95e-02	-	3.23e-02	-
1/32	9.97e-02	1.00	9.94e-03	1.57	1.06e-02	1.61
1/64	4.98e-02	1.00	3.53e-03	1.50	3.08e-03	1.78
1/128	2.49e-02	1.00	1.19e-03	1.56	1.05e-03	1.55
1/256	1.25e-02	1.00	4.33e-04	1.46	3.85e-04	1.45
1/512	6.23e-03	1.00	1.56e-04	1.47	1.38e-04	1.48
1/1024	3.12e-03	1.00	5.51e-05	1.50	4.85e-05	1.51

Table 4
Numerical results for Example 5.1 with $\beta_1 = 100000, \beta_2 = 1$.

h	De	Order	$D^i e$	Order	$D^r e$	Order
1/16	4.19e-02	-	2.62e-02	-	2.15e-02	-
1/32	2.13e-02	0.98	9.99e-03	1.39	8.54e-03	1.33
1/64	1.06e-02	1.00	3.54e-03	1.50	3.10e-03	1.46
1/128	5.33e-03	1.00	1.25e-03	1.50	1.12e-03	1.46
1/256	2.66e-03	1.00	4.33e-04	1.52	3.84e-04	1.55
1/512	1.33e-03	1.00	1.52e-04	1.51	1.37e-04	1.48
1/1024	6.66e-04	1.00	5.41e-05	1.49	4.65e-05	1.56

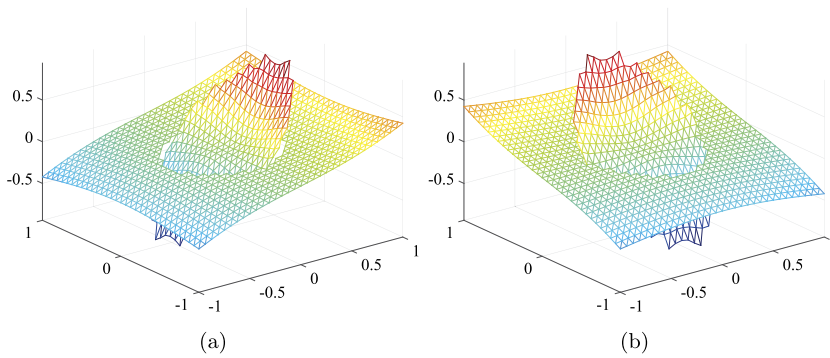


Fig. 3. Plots of recovered gradient for Example 5.1: (a) x-component; (b) y-component.

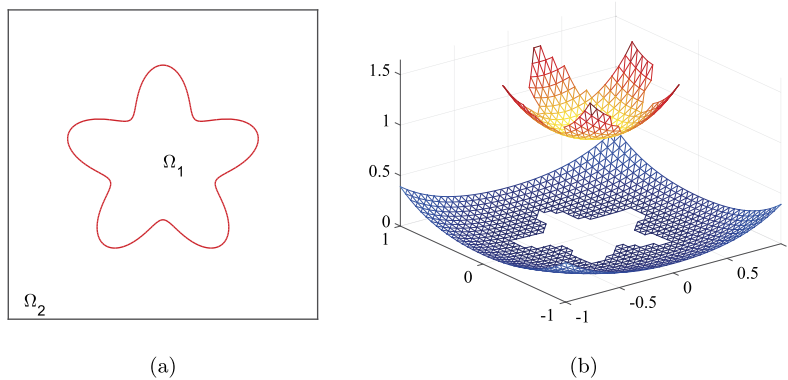


Fig. 4. Plots for Example 5.2: (a) plot of the interface; (b) plot of numerical solution.

$$r = \frac{1}{2} + \frac{\sin(5\theta)}{7}.$$

It contains both convex and concave parts, as demonstrated in Fig. 4a. The diffusion coefficient is piecewise constant with $\beta_1 = 1$ and $\beta_2 = 10$. The right-hand side function f in (2.1a) is chosen to match the exact solution

$$u(x, y) = \begin{cases} e^{(x^2+y^2)}, & \text{if } (x, y) \in \Omega_1 \\ 0.1(x^2 + y^2)^2 - 0.01 \ln(2\sqrt{x^2 + y^2}), & \text{if } (x, y) \in \Omega_2, \end{cases}$$

Table 5
Numerical results for Example 5.2.

h	De	Order	$D^i e$	Order	$D^r e$	Order
1/16	8.86e-02	-	5.81e-02	-	3.74e-02	-
1/32	3.90e-02	1.19	1.50e-02	1.95	1.19e-02	1.65
1/64	1.90e-02	1.04	4.37e-03	1.78	3.57e-03	1.74
1/128	9.48e-03	1.00	1.57e-03	1.48	1.29e-03	1.47
1/256	4.74e-03	1.00	5.63e-04	1.48	4.72e-04	1.45
1/512	2.37e-03	1.00	2.00e-04	1.50	1.71e-04	1.47
1/1024	1.18e-03	1.00	7.06e-05	1.50	6.62e-05	1.37

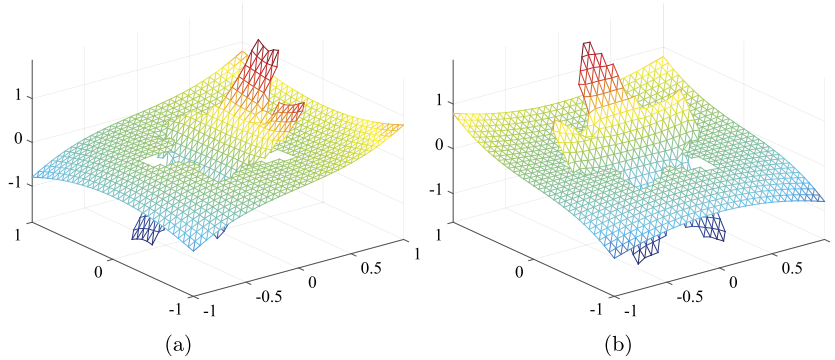


Fig. 5. Plots of recovered gradient for Example 5.2 on the initial mesh: (a) x-component; (b) y-component.

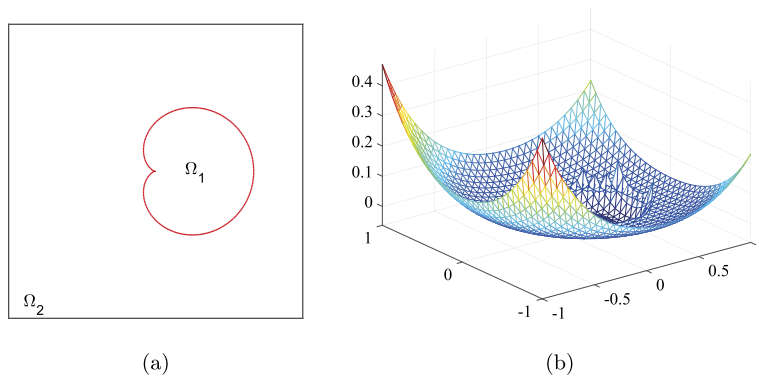


Fig. 6. Plots for Example 5.3: (a) plot of the interface; (b) plot of numerical solution.

and the jump conditions (2.1c)–(2.1d) are provided by the exact solution.

In Fig. 4b, we plot the numerical solution on the initial mesh which clearly indicates the non-homogeneous jump in function value. We show the numerical results in Table 5. As expected, we observe the first-order convergence for the gradient of finite element solution. For the recovered gradient, $\mathcal{O}(h^{1.5})$ convergence is observed, which is in agreement with Theorem 4.2. The recovered gradient on the initial mesh is visualized in Fig. 5.

Example 5.3. In this example, we consider the following nonlinear interface problem with homogeneous jump conditions

$$-\nabla \cdot (\beta \nabla u) + \sin(u) = f, \quad z \text{ in } \Omega \setminus \Gamma.$$

The interface curve Γ is the zero level of the function

$$\phi(x, y) = (3(x^2 + y^2) - x)^2 - x^2 - y^2,$$

as shown Fig. 6a. We choose the exact solution $u(x, y) = \phi(x, y)/\beta(x, y)$, where

$$\beta(x, y) = \begin{cases} xy + 3 & \text{if } (x, y) \in \Omega_1, \\ 100 & \text{if } (x, y) \in \Omega_2. \end{cases}$$

The right hand side function f and boundary condition are determined by the exact solution.

Table 6
Numerical results for Example 5.3.

h	De	Order	$D^i e$	Order	$D^r e$	Order
1/16	5.76e-02	–	3.89e-02	–0	2.70e-02	–
1/32	2.94e-02	0.97	1.41e-02	1.46	1.00e-02	1.43
1/64	1.48e-02	0.99	5.32e-03	1.41	3.94e-03	1.35
1/128	7.44e-03	0.99	1.86e-03	1.51	1.41e-03	1.48
1/256	3.72e-03	1.00	6.77e-04	1.46	5.18e-04	1.44
1/512	1.86e-03	1.00	2.38e-04	1.51	1.82e-04	1.50
1/1024	9.32e-04	1.00	8.44e-05	1.49	6.52e-05	1.48

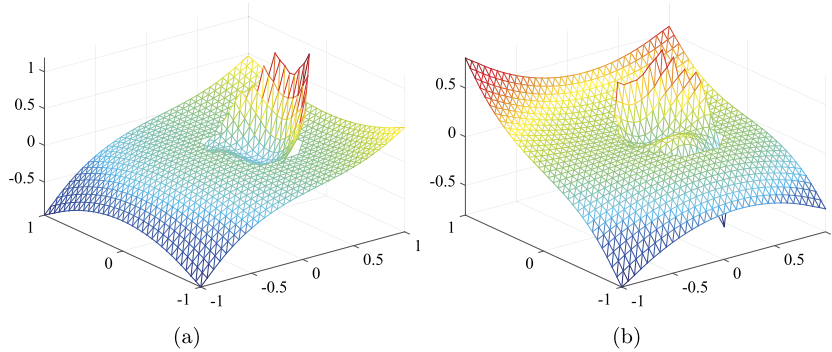


Fig. 7. Plots of recovered gradient for Example 5.3 on the initial mesh. (a) x-component; (b) y-component.

We solve the discretized nonlinear problem by Newton’s method. In Fig. 6b, we plot the numerical solution on the initial mesh. The numerical results are given in Table 6. Note that interface is not even Lipschitz-continuous and has a singular point at the origin. Even though in that case, we observe the same superconvergence results as in linear interface problems. The recovered gradient on the initial mesh is visualized in Fig. 7.

Example 5.4. In this example, we consider the interface problem with complex geometrical structure as in [48]. The interface in polar coordinates is given by

$$r = 0.40178(1 + \cos(2\theta) \sin(6\theta)) \cos(\theta).$$

The interface and subdomains are plotted in Fig. 4a. The coefficient function is

$$\beta(x, y) = \begin{cases} (x^2 - y^2 - 7)/7, & (x, y) \in \Omega_1, \\ (xy + 2)/5, & (x, y) \in \Omega_2; \end{cases}$$

and the exact function is

$$u(x, y) = \begin{cases} \sin(x + y) + \cos(x + y) + 1, & (x, y) \in \Omega_1, \\ x + y + 1, & (x, y) \in \Omega_2. \end{cases}$$

As plotted in Fig. 8a, the interface contains complex geometrical structure. To guarantee the Assumption 2.2, we need an extremely fine mesh. It would increase the computational cost. To reduce the computational cost, we propose an adaptive strategy to generate an initial unfitted mesh. Here we use the curvature-based *a posteriori* estimator to guide the refinement of the mesh as in [56]. Different from the mesh generated in [56], the resulted mesh is an unfitted mesh and all triangles are perfect right triangles.

Fig. 8b plots the generated initial unfitted mesh. It is easy to see that the mesh is refined around the part of the interface with high curvature. The other four levels of unfitted meshes are obtained by uniform refinement. The numerical results are summarized in Table 7. Note that in Table 7, convergence rates are listed with respect to the degree of freedom (DOF). The corresponding convergent rates with respect to the mesh size h are double of what we present in Table 7. The gradient of finite element solution converges to the exact gradient at the rate of $\mathcal{O}(h)$ while the recovered gradient superconverges at the rate of $\mathcal{O}(h^{1.5})$. Additionally, the predicted supercloseness is observed in the numerical experiment.

Example 5.5. In this example, we consider the interface problem as in [6,56]. The interface in parametric form is given by

$$\begin{cases} x(t) = r(t) \cos(\theta(t)), \\ y(t) = r(t) \sin(\theta(t)); \end{cases}$$

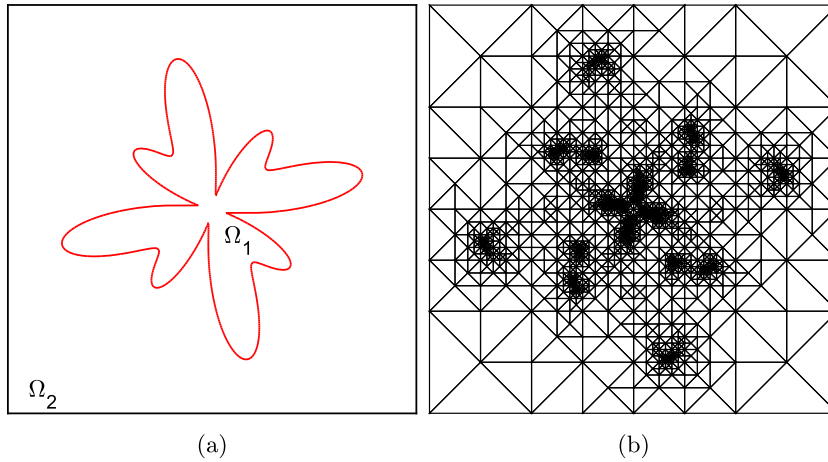


Fig. 8. Plots for Example 5.4: (a) plot of the interface; (b) initial unfitted mesh.

Table 7
Numerical results for Example 5.4.

DOF	De	Order	$D^i e$	Order	$D^r e$	Order
2573	2.49e-02	–	1.32e-02	–	8.68e-03	–
10265	1.29e-02	0.48	4.42e-03	0.79	3.20e-03	0.72
41009	6.57e-03	0.49	1.56e-03	0.75	1.25e-03	0.68
163937	3.30e-03	0.50	5.09e-04	0.81	4.46e-04	0.74
655553	1.66e-03	0.50	1.74e-04	0.77	1.59e-04	0.74
2621825	8.28e-04	0.50	5.92e-05	0.78	5.48e-05	0.77

where

$$\theta(t) = t + \sin(4t), \quad r(t) = 0.60125 + 0.24012 \cos(4t + \pi/2).$$

The coefficient function is

$$\beta(x, y) = \begin{cases} 4 + \sin(x + y), & (x, y) \in \Omega_1, \\ 10 + x^2 + y^2, & (x, y) \in \Omega_2; \end{cases}$$

and the exact solution is

$$u(x, y) = \begin{cases} \sin(x) \cos(y), & (x, y) \in \Omega_1, \\ 1 - x^2 - y^2, & (x, y) \in \Omega_2. \end{cases}$$

The interface Γ , shown in Fig. 9a, contains complex geometrical structure. We use the same algorithm as in Example 5.3 to generate an initial unfitted mesh which is plotted in Fig. 9b. Table 8 lists the numerical results. Clearly, we observe the desired optimal convergence and superconvergence rates.

Example 5.6. In this example, we consider the interface problem as in [39,56]. The interface Γ in parametric form is defined by

$$\begin{cases} x(t) = r(\theta) \cos(\theta) + x_c, \\ y(t) = r(\theta) \sin(\theta) + y_c; \end{cases}$$

where $r(\theta) = r_0 + r_1 \sin(\omega\theta)$, $0 \leq \theta < 2\pi$.

In this test, we take $r_0 = 0.4$, $r_1 = 0.2$, $\omega = 20$, and $x_c = y_c = 0.02\sqrt{5}$. The coefficient β is a piecewise constant with $\beta_1 = 1$ and $\beta_2 = 10$. The exact function is

$$u(x, y) = \begin{cases} r^2/\beta_1, & (x, y) \in \Omega_1, \\ (r^4 - 0.1 \log(2r))/\beta_2, & (x, y) \in \Omega_2. \end{cases}$$

The interface Γ is plotted in Fig. 10a and the adaptively refined initial mesh is shown in Fig. 10b. The numerical results are given in Table 9. The observed results confirm the first-order convergence rate as predicted by Theorem 2.6. For the errors De^i and De^r , $\mathcal{O}(h^{1.8})$ order decaying rates can be observed which are better than our theoretical results. Compared

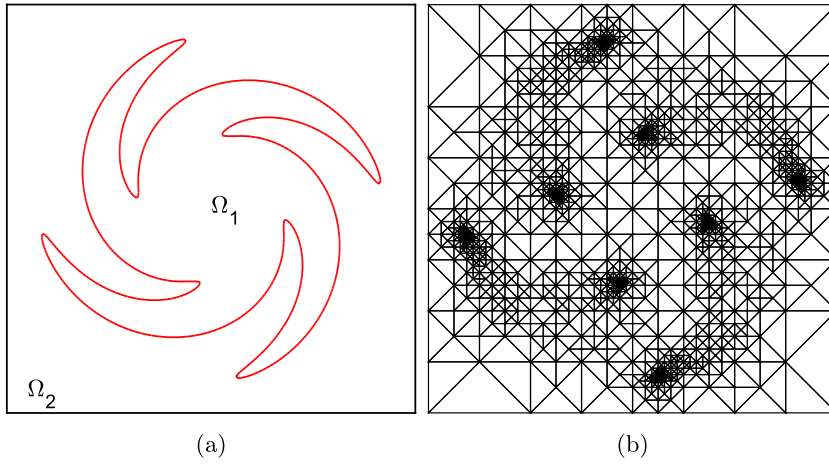


Fig. 9. Plots for Example 5.5: (a) plot of the interface; (b) initial unfitted mesh.

Table 8
Numerical results for Example 5.5.

DOF	De	Order	$D^i e$	Order	$D^f e$	Order
1381	2.14e-01	–	9.04e-02	–	8.01e-02	–
5489	1.12e-01	0.47	2.51e-02	0.93	2.02e-02	1.00
21889	5.67e-02	0.49	7.60e-03	0.86	6.65e-03	0.80
87425	2.85e-02	0.50	2.32e-03	0.86	2.11e-03	0.83
349441	1.42e-02	0.50	7.29e-04	0.83	6.99e-04	0.80
1397249	7.12e-03	0.50	2.43e-04	0.79	2.39e-04	0.78

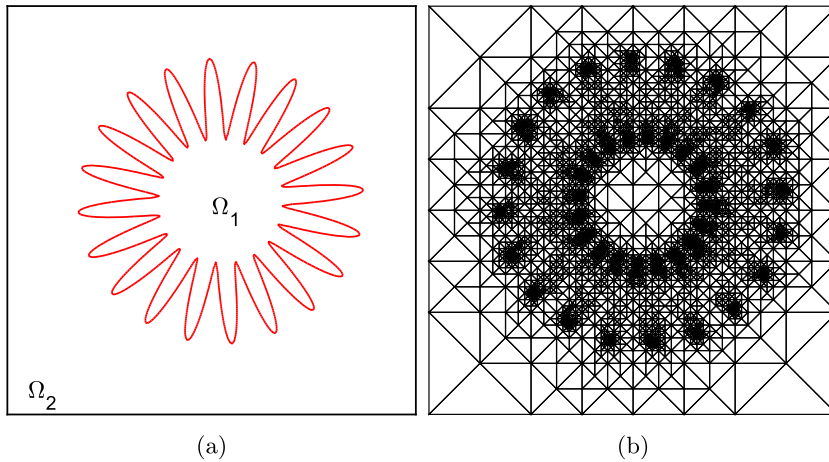


Fig. 10. Plots for Example 5.6: (a) plot of the interface; (b) initial unfitted mesh.

Table 9
Numerical results for Example 5.6.

DOF	De	Order	$D^i e$	Order	$D^f e$	Order
6514	1.30e-01	–	5.36e-02	–	4.39e-02	–
26027	6.70e-02	0.48	1.53e-02	0.91	1.58e-02	0.74
104053	3.39e-02	0.49	4.23e-03	0.93	4.74e-03	0.87
416105	1.70e-02	0.50	1.17e-03	0.93	1.32e-03	0.92
1664209	8.51e-03	0.50	3.26e-04	0.92	3.72e-04	0.91
6656417	4.25e-03	0.50	9.26e-05	0.91	9.97e-05	0.95

to the numerical results using a body-fitted mesh in [56], we achieve the same accuracy by using an unfitted mesh with about one sixth of the total mesh grid points.

6. Conclusion

In this paper, we propose a new gradient recovery technique based on the Nitsche's method. Compared to our previous works [22,23,26], it avoids the loss of accuracy of gradient near the interface caused by skinny triangles. By proving the supercloseness result for the Nitsche's method, we are able to show that the recovered gradient is superconvergent to the exact gradient. As a byproduct, we propose a curvature estimator based adaptive algorithm to generate initial unfitted triangulations for the elliptic interface problems with complex geometry, which greatly reduces the computational cost as illustrated in Examples 5.4, 5.5 and 5.6. The future work is planned in several different directions: firstly, we will extend the study into three dimension problems; secondly, we will consider other type equations like elastic interface problems and wave propagation problems in heterogeneous media; thirdly, we will combine the curvature estimator and the recovery-based *a posteriori* error estimator to derive adaptive algorithms for the complex interface problems.

Acknowledgements

This work was partially supported by the NSF grants DMS-1418936 and DMS-1107291.

References

- [1] M. Ainsworth, J.T. Oden, *A Posteriori Error Estimation in Finite Element Analysis*, Pure and Applied Mathematics, Wiley-Interscience, John Wiley & Sons, New York, ISBN 0-471-29411-X, 2000.
- [2] C. Annavarapu, M. Hautefeuille, J.E. Dolbow, A robust Nitsche's formulation for interface problems, *Comput. Methods Appl. Mech. Eng.* (ISSN 0045-7825) 225 (228) (2012) 44–54.
- [3] I. Babuška, The finite element method for elliptic equations with discontinuous coefficients, *Computing (Arch. Elektron. Rechnen)* 5 (1970) 207–213.
- [4] R.E. Bank, J. Xu, Asymptotically exact *a posteriori* error estimators, II: general unstructured grids, *SIAM J. Numer. Anal.* (ISSN 0036-1429) 41 (6) (2003) 2313–2332.
- [5] R. Becker, E. Burman, P. Hansbo, A Nitsche extended finite element method for incompressible elasticity with discontinuous modulus of elasticity, *Comput. Methods Appl. Mech. Eng.* (ISSN 0045-7825) 198 (41–44) (2009) 3352–3360.
- [6] J. Bedrossian, J.H. von Brecht, S. Zhu, E. Sifakis, J.M. Teran, A second order virtual node method for elliptic problems with interfaces and irregular domains, *J. Comput. Phys.* (ISSN 0021-9991) 229 (18) (2010) 6405–6426.
- [7] T. Belytschko, T. Black, A finite element method for crack growth without remeshing, *Int. J. Numer. Methods Eng.* (ISSN 0029-5981) 45 (5) (1999) 601–620.
- [8] J.H. Bramble, J.T. King, A finite element method for interface problems in domains with smooth boundaries and interfaces, *Adv. Comput. Math.* (ISSN 1019-7168) 6 (2) (1997) 109–138, 1996.
- [9] S.C. Brenner, L.R. Scott, *The Mathematical Theory of Finite Element Methods*, third edition, *Texts in Applied Mathematics*, vol. 15, Springer, New York, ISBN 978-0-387-75933-3, 2008.
- [10] E. Burman, P. Hansbo, Fictitious domain finite element methods using cut elements, II: a stabilized Nitsche method, *Appl. Numer. Math.* (ISSN 0168-9274) 62 (4) (2012) 328–341.
- [11] E. Burman, P. Hansbo, Fictitious domain methods using cut elements, III: a stabilized Nitsche method for Stokes' problem, *Modél. Math. Anal. Numér.* (ISSN 0764-583X) 48 (3) (2014) 859–874.
- [12] E. Burman, S. Claus, P. Hansbo, M.G. Larson, A. Massing, CutFEM: discretizing geometry and partial differential equations, *Int. J. Numer. Methods Eng.* (ISSN 0029-5981) 104 (7) (2015) 472–501.
- [13] L. Chen, J. Xu, A posteriori error estimator by post-processing, in: Jinchao Xu, Tao Tang (Eds.), *Adaptive Computations: Theory and Algorithms*, Science Press, Beijing, 2007, pp. 34–67.
- [14] Z. Chen, J. Zou, Finite element methods and their convergence for elliptic and parabolic interface problems, *Numer. Math.* (ISSN 0029-599X) 79 (2) (1998) 175–202.
- [15] S.-H. Chou, An immersed linear finite element method with interface flux capturing recovery, *Discrete Contin. Dyn. Syst., Ser. B* (ISSN 1531-3492) 17 (7) (2012) 2343–2357.
- [16] S.H. Chou, C. Attanayake, Flux recovery and superconvergence of quadratic immersed interface finite elements, *Int. J. Numer. Anal. Model.* (ISSN 1705-5105) 14 (1) (2017) 88–102.
- [17] P.G. Ciarlet, *The Finite Element Method for Elliptic Problems*, *Classics in Applied Mathematics*, vol. 40, Society for Industrial and Applied Mathematics (SIAM), Philadelphia, PA, ISBN 0-89871-514-8, 2002, reprint of the 1978 original [North-Holland, Amsterdam; MR0520174 (58 #25001)].
- [18] L.C. Evans, *Partial Differential Equations*, second edition, *Graduate Studies in Mathematics*, vol. 19, American Mathematical Society, Providence, RI, ISBN 978-0-8218-4974-3, 2010.
- [19] T.-P. Fries, T. Belytschko, The extended/generalized finite element method: an overview of the method and its applications, *Int. J. Numer. Methods Eng.* (ISSN 0029-5981) 84 (3) (2010) 253–304, <https://doi.org/10.1002/nme.2914>.
- [20] F. Gibou, R.P. Fedkiw, S. Osher, A review of level-set methods and some recent applications, *J. Comput. Phys.* (ISSN 0021-9991) 353 (2018) 82–109.
- [21] A. Guittet, M. Lepilliez, S. Tanguy, F. Gibou, Solving elliptic problems with discontinuities on irregular domains—the Voronoi interface method, *J. Comput. Phys.* (ISSN 0021-9991) 298 (2015) 747–765.
- [22] H. Guo, X. Yang, Gradient recovery for elliptic interface problem, I: body-fitted mesh, arXiv:1607.05898 [math.NA], 2016.
- [23] H. Guo, X. Yang, Gradient recovery for elliptic interface problem, II: immersed finite element methods, *J. Comput. Phys.* (ISSN 0021-9991) 338 (2017) 606–619.
- [24] H. Guo, X. Yang, Polynomial preserving recovery for high frequency wave propagation, *J. Sci. Comput.* (ISSN 0885-7474) 71 (2) (2017) 594–614.
- [25] H. Guo, Z. Zhang, Gradient recovery for the Crouzeix–Raviart element, *J. Sci. Comput.* (ISSN 0885-7474) 64 (2) (2015) 456–476.
- [26] H. Guo, X. Yang, Z. Zhang, Superconvergence of partially penalized immersed finite element methods, *IMA J. Numer. Anal.* (ISSN 0272-4979) (2017), <https://doi.org/10.1093/imanum/drx053>.
- [27] A. Hansbo, P. Hansbo, An unfitted finite element method, based on Nitsche's method, for elliptic interface problems, *Comput. Methods Appl. Mech. Eng.* (ISSN 0045-7825) 191 (47–48) (2002) 5537–5552.

- [28] A. Hansbo, P. Hansbo, A finite element method for the simulation of strong and weak discontinuities in solid mechanics, *Comput. Methods Appl. Mech. Eng.* (ISSN 0045-7825) 193 (33–35) (2004) 3523–3540.
- [29] A. Hansbo, P. Hansbo, M.G. Larson, A finite element method on composite grids based on Nitsche's method, *Modél. Math. Anal. Numér.* (ISSN 0764-583X) 37 (3) (2003) 495–514.
- [30] P. Hansbo, Nitsche's method for interface problems in computational mechanics, *GAMM-Mitt.* (ISSN 0936-7195) 28 (2) (2005) 183–206, <https://doi.org/10.1002/gamm.201490018>.
- [31] P. Hansbo, M.G. Larson, S. Zahedi, A cut finite element method for a Stokes interface problem, *Appl. Numer. Math.* (ISSN 0168-9274) 85 (2014) 90–114.
- [32] S. Hou, X.-D. Liu, A numerical method for solving variable coefficient elliptic equation with interfaces, *J. Comput. Phys.* (ISSN 0021-9991) 202 (2) (2005) 411–445.
- [33] S. Hou, W. Wang, L. Wang, Numerical method for solving matrix coefficient elliptic equation with sharp-edged interfaces, *J. Comput. Phys.* (ISSN 0021-9991) 229 (19) (2010) 7162–7179.
- [34] S. Hou, P. Song, L. Wang, H. Zhao, A weak formulation for solving elliptic interface problems without body fitted grid, *J. Comput. Phys.* (ISSN 0021-9991) 249 (2013) 80–95.
- [35] T.Y. Hou, X.-H. Wu, Y. Zhang, Removing the cell resonance error in the multiscale finite element method via a Petrov–Galerkin formulation, *Commun. Math. Sci.* (ISSN 1539-6746) 2 (2) (2004) 185–205.
- [36] H. Ji, J. Chen, Z. Li, A symmetric and consistent immersed finite element method for interface problems, *J. Sci. Comput.* (ISSN 0885-7474) 61 (3) (2014) 533–557.
- [37] R.J. LeVeque, Z. Li, The immersed interface method for elliptic equations with discontinuous coefficients and singular sources, *SIAM J. Numer. Anal.* (ISSN 0036-1429) 31 (4) (1994) 1019–1044.
- [38] Z. Li, The immersed interface method using a finite element formulation, *Appl. Numer. Math.* (ISSN 0168-9274) 27 (3) (1998) 253–267.
- [39] Z. Li, A fast iterative algorithm for elliptic interface problems, *SIAM J. Numer. Anal.* (ISSN 0036-1429) 35 (1) (1998) 230–254.
- [40] Z. Li, K. Ito, The immersed interface method, in: *Numerical Solutions of PDEs Involving Interfaces and Irregular Domains*, in: *Frontiers in Applied Mathematics*, vol. 33, Society for Industrial and Applied Mathematics (SIAM), Philadelphia, PA, ISBN 0-89871-609-8, 2006.
- [41] Z. Li, T. Lin, X. Wu, New Cartesian grid methods for interface problems using the finite element formulation, *Numer. Math.* (ISSN 0029-599X) 96 (1) (2003) 61–98.
- [42] Z. Li, T. Lin, Y. Lin, R.C. Rogers, An immersed finite element space and its approximation capability, *Numer. Methods Partial Differ. Equ.* (ISSN 0749-159X) 20 (3) (2004) 338–367.
- [43] Z. Li, H. Ji, X. Chen, Accurate solution and gradient computation for elliptic interface problems with variable coefficients, *SIAM J. Numer. Anal.* 55 (2) (2017) 570–597.
- [44] T. Lin, Y. Lin, X. Zhang, Partially penalized immersed finite element methods for elliptic interface problems, *SIAM J. Numer. Anal.* (ISSN 0036-1429) 53 (2) (2015) 1121–1144, <https://doi.org/10.1137/130912700>.
- [45] X.-D. Liu, R.P. Fedkiw, M. Kang, A boundary condition capturing method for Poisson's equation on irregular domains, *J. Comput. Phys.* (ISSN 0021-9991) 160 (1) (2000) 151–178.
- [46] N. Moës, J. Dolbow, T. Belytschko, A finite element method for crack growth without remeshing, *Int. J. Numer. Methods Eng.* (ISSN 0029-5981) 51 (3) (2001) 293–313.
- [47] L. Mu, J. Wang, G. Wei, X. Ye, S. Zhao, Weak Galerkin methods for second order elliptic interface problems, *J. Comput. Phys.* (ISSN 0021-9991) 250 (2013) 106–125.
- [48] L. Mu, J. Wang, X. Ye, S. Zhao, A new weak Galerkin finite element method for elliptic interface problems, *J. Comput. Phys.* (ISSN 0021-9991) 325 (2016) 157–173.
- [49] A. Naga, Z. Zhang, A posteriori error estimates based on the polynomial preserving recovery, *SIAM J. Numer. Anal.* (ISSN 0036-1429) 42 (4) (2004) 1780–1800 (electronic).
- [50] A. Naga, Z. Zhang, The polynomial-preserving recovery for higher order finite element methods in 2D and 3D, *Discrete Contin. Dyn. Syst., Ser. B* (ISSN 1531-3492) 5 (3) (2005) 769–798.
- [51] J. Nitsche, Über ein Variationsprinzip zur Lösung von Dirichlet-Problemen bei Verwendung von Teilräumen, die keinen Randbedingungen unterworfen sind, *Abh. Math. Semin. Univ. Hamb.* (ISSN 0025-5858) 36 (1971) 9–15, collection of articles dedicated to Lothar Collatz on his sixtieth birthday.
- [52] C.S. Peskin, Numerical analysis of blood flow in the heart, *J. Comput. Phys.* (ISSN 0021-9991) 25 (3) (1977) 220–252.
- [53] C.S. Peskin, The immersed boundary method, *Acta Numer.* (ISSN 0962-4929) 11 (2002) 479–517.
- [54] F. Qin, Z. Wang, Z. Ma, Z. Li, Accurate gradient computations at interfaces using finite element methods, arXiv:1703.00093 [math.NA], 2017.
- [55] E. Wadbro, S. Zahedi, G. Kreiss, M. Berggren, A uniformly well-conditioned, unfitted Nitsche method for interface problems, *BIT* (ISSN 0006-3835) 53 (3) (2013) 791–820.
- [56] H. Wei, L. Chen, Y. Huang, B. Zheng, Adaptive mesh refinement and superconvergence for two-dimensional interface problems, *SIAM J. Sci. Comput.* (ISSN 1064-8275) 36 (4) (2014) A1478–A1499.
- [57] J. Xu, Error estimates of the finite element method for the 2nd order elliptic equations with discontinuous coefficients, *J. Xiangtan Univ.* 1 (1982) 1–5.
- [58] J. Xu, Z. Zhang, Analysis of recovery type a posteriori error estimators for mildly structured grids, *Math. Comput.* (ISSN 0025-5718) 73 (247) (2004) 1139–1152 (electronic).
- [59] Z. Zhang, Recovery techniques in finite element methods, in: Jinchao Xu, Tao Tang (Eds.), *Adaptive Computations: Theory and Algorithms*, Science Press, Beijing, 2007, pp. 297–365.
- [60] Z. Zhang, A. Naga, A new finite element gradient recovery method: superconvergence property, *SIAM J. Sci. Comput.* (ISSN 1064-8275) 26 (4) (2005) 1192–1213 (electronic).
- [61] X. Zheng, J. Lowengrub, An interface-fitted adaptive mesh method for elliptic problems and its application in free interface problems with surface tension, *Adv. Comput. Math.* (ISSN 1019-7168) 42 (5) (2016) 1225–1257.
- [62] Y.C. Zhou, G.W. Wei, On the fictitious-domain and interpolation formulations of the matched interface and boundary (MIB) method, *J. Comput. Phys.* (ISSN 0021-9991) 219 (1) (2006) 228–246.
- [63] Y.C. Zhou, S. Zhao, M. Feig, G.W. Wei, High order matched interface and boundary method for elliptic equations with discontinuous coefficients and singular sources, *J. Comput. Phys.* (ISSN 0021-9991) 213 (1) (2006) 1–30.
- [64] O.C. Zienkiewicz, J.Z. Zhu, The superconvergent patch recovery and a posteriori error estimates. I: the recovery technique, *Int. J. Numer. Methods Eng.* (ISSN 0029-5981) 33 (7) (1992) 1331–1364.
- [65] O.C. Zienkiewicz, J.Z. Zhu, The superconvergent patch recovery and a posteriori error estimates, II: error estimates and adaptivity, *Int. J. Numer. Methods Eng.* (ISSN 0029-5981) 33 (7) (1992) 1365–1382.
- [66] O.C. Zienkiewicz, R.L. Taylor, J.Z. Zhu, *The Finite Element Method: Its Basis and Fundamentals*, seventh edition, Elsevier/Butterworth Heinemann, Amsterdam, ISBN 978-1-85617-633-0, 2013.